applied sciences

MDPI

Article

Diketo-Pyrrolo Pyrrole-Based Acceptor-Acceptor Copolymers with Deep HOMO and LUMO Levels Absorbing in the Near Infrared

Wissem Khelifi [1], Hussein Awada [1], Sylvie Blanc [1], Gilles Henri Roche [2], Lionel Hirsch [2], Bassey Oboho [3], Frédéric Castet [3], Antoine Bousquet [1,*] and Christine Lartigau-Dagron [1,*]

[1] Universite de Pau et des Pays de l'Adour, E2S UPPA, CNRS, IPREM, 64053 Pau, France; khelifi.wissem@live.fr (W.K.); hussein-awada1@hotmail.com (H.A.); sylvie.blanc@univ-pau.fr (S.B.)
[2] Univ. Bordeaux, IMS, CNRS, UMR 5218, Bordeaux INP, ENSCBP, 33405 Talence, France; gilles.roche@u-bordeaux.fr (G.H.R.); lionel.hirsch@ims-bordeaux.fr (L.H.)
[3] Univ. Bordeaux, CNRS, Bordeaux INP, ISM, UMR 5255, 33405 Talence, France; b.oboho@lboro.ac.uk (B.O.); frederic.castet@u-bordeaux.fr (F.C.)
* Correspondence: antoine.bousquet@univ-pau.fr (A.B.); christine.lartigau-dagron@univ-pau.fr (C.L.-D.)

Featured Application: Copolymers with an absorption in the near infra-red have potential applications in organic photodetectors.

Abstract: A series of acceptor-acceptor (A-A') alternated copolymers based on dithienodiketopyrrolo pyrrole were synthesized by copolymerizing it with itself and other different electron-poor monomers. The experimental and computed optoelectronic properties of four DPP-based copolymers, P(DPP-DPP) (with linear and branched chains), copolymer with diazapentalene P(DPP-DAP) and also with dioxothienopyrrolebenzodifurandione P(DPP-BTPBF), as well as thermal characterizations were described. UV-visible spectrophotometry and cyclic voltammetry were used to estimate the optical and electrochemical bandgaps, and were found as very small: 1.3, 1.0, and 0.9 eV for P(DPP-DPP), P(DPP-DAP), and P(DPP-BTPBF), respectively. The BTPBF unit allowed a strong reduction of the bandgap, leading to a broad absorption in the visible and near infra-red regions from 650 to 1450 nm. These results were compared to analogous donor-acceptor (D-A) copolymers previously reported, in which DPP is replaced by DTS, P(DTS-DPP), P(DTS-DAP), and P(DTS-BTPBF). The same trend was observed. By comparing A-A' to D-A' copolymers analogues, it was shown that the bandgap remained the same while both HOMO and LUMO levels were lowered by roughly 0.2 eV.

Keywords: copolymer; near infra-red; low bandgap

Citation: Khelifi, W.; Awada, H.; Blanc, S.; Roche, G.H.; Hirsch, L.; Oboho, B.; Castet, F.; Bousquet, A.; Lartigau-Dagron, C. Diketo-Pyrrolo Pyrrole-Based Acceptor-Acceptor Copolymers with Deep HOMO and LUMO Levels Absorbing in the Near Infrared. *Appl. Sci.* **2022**, *12*, 4494. https://doi.org/10.3390/app12094494

Academic Editor: Sang Hyuk Im

Received: 29 March 2022
Accepted: 25 April 2022
Published: 28 April 2022

1. Introduction

The vast majority of conjugated polymers dedicated to organic electronics are developed using the donor-acceptor (D-A) strategy, which consists of combining electron-rich (D) and electron-poor (A) units, and in varying their nature through chemical design in order to finely tune their bandgap [1]. Generally, D-A copolymers were mainly used as donor materials (p-type) combined with fullerene acceptors (n-type) for organic solar cells (OSCs). However, since fullerene derivatives suffer from limitations like weak absorption and low stability due to dimerization (burn-in) and unstable morphology [2–4], non fullerene acceptors (NFAs) were developed for organic electronic devices [5,6]. With the need of reducing more and more the bandgap, n-type polymers exhibiting a LUMO level at −4 eV have been tested for integration in organic field-effect transistors (OFETs) and OSCs [7–10]. In this context, a variety of D-A acceptor polymers based on benzothiadiazole (BT), dithienodiketopyrrolo pyrrole (DPP), thienopyrroledione (TPD), naphthalene diimide (NDI), and perylene diimide (PDI) have been developed [11–16]. Even if they did not

provide the same level of performances in OSCs as fullerene-based devices, the use of n-type polymers is of great interest owing to the possibility of tuning their optoelectronic properties to optimize their light-harvesting capability and improve their stability [17]. Among n-type polymers, those based on naphthalene diimide (NDI) and perylene diimide (PDI) are an important series that show good performances in all-polymer solar cells [18–22]. Performances of OSCs combining PDI-based D-A acceptor polymers with adequate p-type polymers achieved power conversion efficiencies (PCE) up to 7% [23]. It has been demonstrated that D-A copolymers based on DPP combined with thiophene or selenophene could exhibit a high photoresponse with a tuneable absorption edge from 950 to 1200 nm, allowing PCE from 2.9% to 5.3% [24]. A recent review reported ultra-narrow-bandgap D-A copolymers for OSCs, mainly based on DPP and isoindigo units that can be used as donor materials [25]. Some D-A copolymers presenting an absorption in the NIR range based on thiadiazoloquinoxaline [26] or on diazapentalene (DAP) units [27] were efficiently used in organic PDs.

Besides D-A copolymers, systems combining two electron-accepting A-A′ units have also been reported. They can afford n-type materials more stable under air and with deeper HOMO levels, as reported by the combination of PDI with fluorenone [28]. Dual-acceptor copolymers based on 2-alkylbenzotriazole and 2,1,3-benzothiadiazole (BT) were reported for OFETs with an electron mobility of 0.01 $cm^2\ V^{-1}\ s^{-1}$ [29], and all-polymer solar cells with a PCE of 0.31% [30]. Benzotriazole was also copolymerized with other electron poor units, such as quinoxaline and benzobisthiadiazole, and were used as n-type copolymers in OSCs showing a PCE of 0.40%. A-A′ copolymers based on isoindigo and BT were also used as acceptor materials in solar cells with a similar PCE (0.47%) [31]. A-A′ copolymers based on PDI and BT provided an efficiency of 0.31% [32]. All these copolymers have an optical absorption in the visible range, and showed low performances in solar cells compared with their D-A analogues. A recent strategy is now being developed to polymerize small molecular acceptors (initially used as NFAs), allowing the preparation of n-type polymers for all-polymer solar cells, with PCE up to 16% [33,34].

Conversely, A-A′ copolymers with very low bandgap absorbing in the NIR range have been scarcely considered. Copolymers combining diketopyrrolopyrole (DPP) and benzo [1,2-c;3,4-c′] bis [1,2,5] thiadiazole (BBT) were obtained with a very low bandgap of 0.65 eV [35]. Used in transistors, they exhibited a clear ambipolar behavior with high n and p-type charge mobilities between 0.5 and 1 $cm^2\ V^{-1}\ s^{-1}$. A-A′ copolymers based on thienoisoindigo (TII) and DPP have also been synthesized, presenting a wide absorption domain ranging between 350 and 2175 nm, and therefore a very low optical bandgap between 1.24 and 0.57 eV. An ambipolar behavior was found when integrated into transistor devices [36]. Another example described the synthesis of a NIR-absorbing A-A′ copolymers combining TII with DPP via direct arylation polymerization, which absorb in the 350–1500 nm range, with calculated optical gaps between 0.91 and 0.82 eV. These different copolymers have also been tested in transistor devices, showing lower charge mobilities for electrons and holes of the order of 10^{-5} $cm^2\ V^{-1}\ s^{-1}$ [37]. Another combination from benzo [1,2-c;3,4-c′;], bis [1,2,5], thiadiazole (BBT), and benzo[c] [1,2,5] thiadiazole (BT), substituted with linear or branched chains, afforded copolymers with a very low bandgap energy (~1.0 eV). Different hole mobilities were obtained attributed to the impact of the side chains on the organization of the polymers in the solid state [38].

Herein, three DPP-based conjugated copolymers with backbones exclusively composed of electron poor units were reported, providing new A-A′ copolymers. The aim was to prepare copolymers with reduced band gaps and lowered HOMO and LUMO levels to acquire more stable polymers under air. DPP was chosen for its facile synthesis and its strong electron affinity, potentially affording polymers with good photovoltaic performance and high hole and electron mobilities [39–42]. The DPP core was polymerized with itself or combined with either DAP or a TII derivative, bis(5-oxothieno[3,2-*b*]pyrrole-6-ylidene)benzodifurandione (BTPBF). DAP and BTPBF were selected since they are strong accepting units and their syntheses are derived from DPP precursor [43] and TII, respec-

tively [44–46]. The optical and electrochemical properties of the A-A′ copolymers were compared to that of analogous D-A copolymers with dithienosilole (DTS) as the electron-rich unit. More precisely, P(DPP-DPP) was compared to P(DTS-DPP), P(DPP-DAP) to P(DTS-DAP), and P(DPP-BTBPF) to P(DTS-BTPBF) (see Figure 1 for structures). The results showed that the comparable D-A′ and A-A′ copolymers (with the same A′) roughly presented the same energy of bandgap, ranging from 1.5 to 0.9 eV, while HOMO and LUMO levels were both slightly lowered. Computational chemistry provided a direct insight into the impact of chemical modifications in these structurally similar systems. DFT calculations have been also compared to previously reported theoretical results on D-A′ copolymers [47].

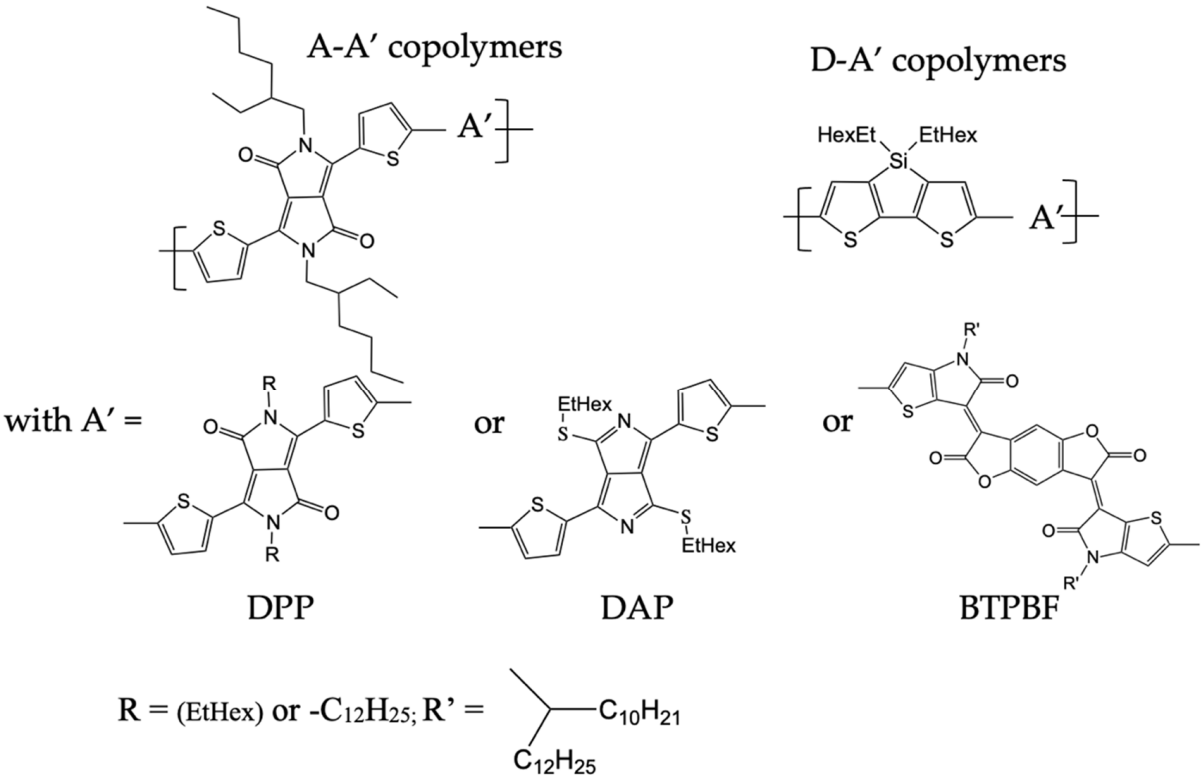

Figure 1. Chemical structures of the A-A′ and D-A′ copolymers considered in this work.

2. Materials and Methods

2.1. Materials

All reactions were performed under dried nitrogen, using flame-dried glassware and conventional Schlenk techniques. Syringes used to transfer reagents and solvents were purged with nitrogen prior to use. Chemicals and reagents were used as received from Aldrich (Saint-Quentin-Fallavier, France), ABCR (Karlsruhe, Germany), and TCI Europe (Zwijndrecht, Belgium) and stored in the glove box. Solvents (Baker, France) were used as received; tetrahydrofuran (THF) and toluene were obtained dried from a solvent dispenser.

Four dibrominated monomers have been used: diketopyrrolopyrrole DPP-eH (branched alkyl chain, ethyl hexyl), DPP-C12 (linear chain with 12 carbons), DAP (2,5-diazapentalene), and BTPBF. The syntheses of the DPP and DAP monomers were previously described by us [43] and the synthesis of the BTPBF monomer was adapted from Cho and co-workers [45]. For the di-stannyl co-monomer, the commercially available DPPeH-distannyl (branched alkyl chain, ethyl hexyl) was chosen. The alternating copolymers P(DPP-DPPeH), P(DPP-DPPC12), P(DPP-DAP), and P(DPP-BTPBF) were synthesized using the Stille coupling.

2.2. Instruments

^{1}H-NMR spectra were recorded on a Bruker (400 MHz) spectrometer; chemical shifts were recorded relative to tetramethylsilane (TMS) with deuterated chloroform ($CDCl_3$) or tetrachloroethane (TCE). Spectra are provided in supplementary information.

UV-Vis-NIR absorption spectra were recorded with a double-beam Cary 5000 UV-Vis-NIR spectrophotometer in steps of 1 nm in the range 350–1800 nm using a 1 cm quartz optical pathlength cell (Hellma).

Cyclic Voltammetry (CV) experiments were performed by using a standard three-electrode electrochemical setup (AUTOLAB PGSTAT 101) consisting of a glassy carbon or a platinum disk as working electrode (2 mm diameter), a platinum foil as counter electrode, and a AgCl/Ag as reference electrode. At the end of each experiment performed in CH_3CN/Bu_4NPF_6 (0.1 M), the standard potential of the ferrocenium/ferrocene couple, $E(Fc^+/Fc)$, was measured, and all potentials were referenced against SCE using a previous determination of $E(Fc^+/Fc)$ = 0.41 V versus SCE in CH_3CN. The solutions were purged with N_2 gas prior to use.

Thermogravimetric analyses (TGA) were performed with a TA-Q50. Aluminum pans were used. Unless specified otherwise, the typical sample weight was ≈3 mg and the typical procedure included a stabilization at 40 °C for 30 min and a heating ramp of 10 °C min^{-1} up to 600 °C.

Differential scanning calorimetry (DSC) measurements were performed with a TA-Q100 in a hermetic aluminum pan. Nitrogen flux was 50 mL s^{-1}. Typical sample weight was ≈5 mg, unless otherwise specified. Typical procedure included a first heating/cooling cycle performed at 10 °C min^{-1} to erase the thermal history of the sample. Then, a ramp of 10 °C min^{-1} was used for heating and cooling cycles, in a temperature range from 0 to 300 °C.

2.3. Computational Methods

The electronic and optical properties of copolymers were computed by using the oligomer approach [43,47–52]. The molecular structures of finite-size $(DA)_n$ oligomers (n = 1–5) were optimized at the density functional theory (DFT) level in the gas phase using the M06-2X exchange-correlation functional [53] (XCF) and the 6-311G(d) basis set (see details in the supporting information). The M06-2X XCF was shown in previous work to reliably describe the structural features of extended π-conjugated systems [54,55].

The vertical excited state energies and oscillator strengths were determined using time-dependent DFT at the same level of approximation. To enable more accurate comparisons with experiments, calculations accounting for solvent effects (chlorobenzene) by means of the integral equation formalism of the polarizable continuum model (IEF-PCM) [56] were also carried out. The $S_0 \rightarrow S_1$ transition energies in the polymer limit were estimated by using the Kuhn's model [57], which describes a polyene chain including *N*-conjugated double bonds as a series of identical coupled oscillators. In this framework, Equation (1) is employed for fitting the transition energies of increasingly large oligomers:

$$E = E_0 \sqrt{1 + D_k \cos\left(\frac{\pi}{N+1}\right)} \quad (1)$$

where E_0 and D_k are adjustable parameters. $E_0 = h\sqrt{k_d/(4\pi^2\mu_d)}$ formally describes the vibration energy of a double bond (k_d and μ_d being the force constant and the reduced mass of the isolated oscillator, respectively), while $D_k = k_s/k_d$ measures the coupling of double bonds through single bonds (with force constant k_s). For the $(A\text{-}A')_n$ systems with A = DPP considered in this study, N = 12n for A′ = DPP or A′ = DAP, and N = 14n for A′ = BTPBF.

3. Results and Discussion

3.1. Synthesis of the A-A′ Copolymers

All syntheses of A-A′ copolymers were based on the Stille copolymerization of distannylated DPP monomer combined with a dibrominated comonomer, either DPP, DAP, or BTPBF (see Scheme 1 for the copolymerization scheme). For DPP as A′, two monomers were used, one with an ethyl hexyl chain (eH) and the other with a linear chain (C12) to discuss the effect of lateral chain on optoelectronic properties. The comonomers were carefully introduced in a stoechiometric ratio to ensure a high conversion, with the catalytic system of tris(dibenzyldeneacetone) dipalladium(0) (Pd_2dba_3) and tri(o-tolyl)phosphine $(o\text{-tol})_3P$ ligand, in anhydrous chlorobenzene. The copolymerizations were first realized as usual at 130 °C under nitrogen, but a precipitation was quickly observed compared with that occurring in D-A systems. Hence, the temperature was lowered to 100 °C and dry toluene was used instead of chlorobenzene to decrease the speed of polymerization, reduce the molar masses of the chains, and ensure the solubility of the final material. After pouring the reaction medium in methanol, the materials were thoroughly purified and fractionated by Soxhlet. Only the chloroform fraction was kept for all the characterizations. The chemical structures of the products, monomers, and polymers were confirmed by ^1H NMR (see the Supplementary Materials, Figures S1−S5).

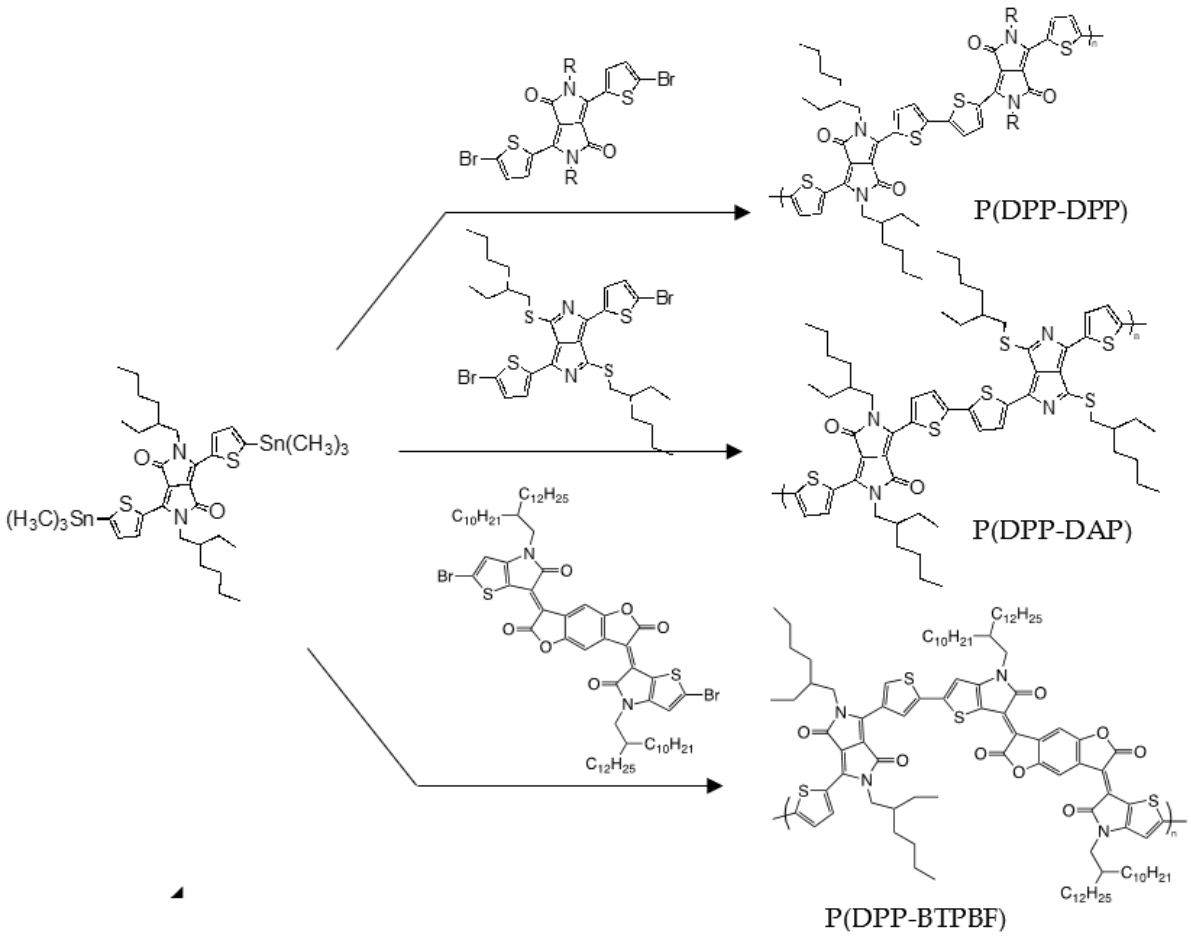

Scheme 1. Stille copolymerization scheme of A-A′ copolymers using $Pd_2(dba)_3/P(o\text{-tol})_3$ in toluene at 100 °C.

3.2. Computational Results

The energies of the highest occupied and lowest unoccupied molecular orbitals (HOMO and LUMO), as well as the HOMO-LUMO gaps of monomers and A-A′ dimeric units are collected in Table S2. Figure 2 illustrates the energy levels and shapes of the

frontier MOs of the DPP-DPP, DPP-DAP, and DPP-BTPBF units issued from the coupling of their constitutive monomers. In the case of the symmetrical DPP-DPP structure, the HOMO and LUMO were spread out evenly throughout each monomer. For A-A′ systems with A = DPP and A′ = DAP or A′ = BTPBF, the HOMOs were primarily localized on the DPP unit, while the LUMOs were mainly spread on the A′ moieties. DPP-DPP had the largest electronic gap of 3.72 eV. When DPP was linked to DAP, the gap reduced to 3.36 eV as a result of the large stabilization of the LUMO. The electronic gap of DPP-BTPBF was close to that of DPP-DAP (3.34 eV) due to the symmetrical downshift (by ~0.1 eV) of the HOMO and LUMO energies with respect to that of DPP-DAP.

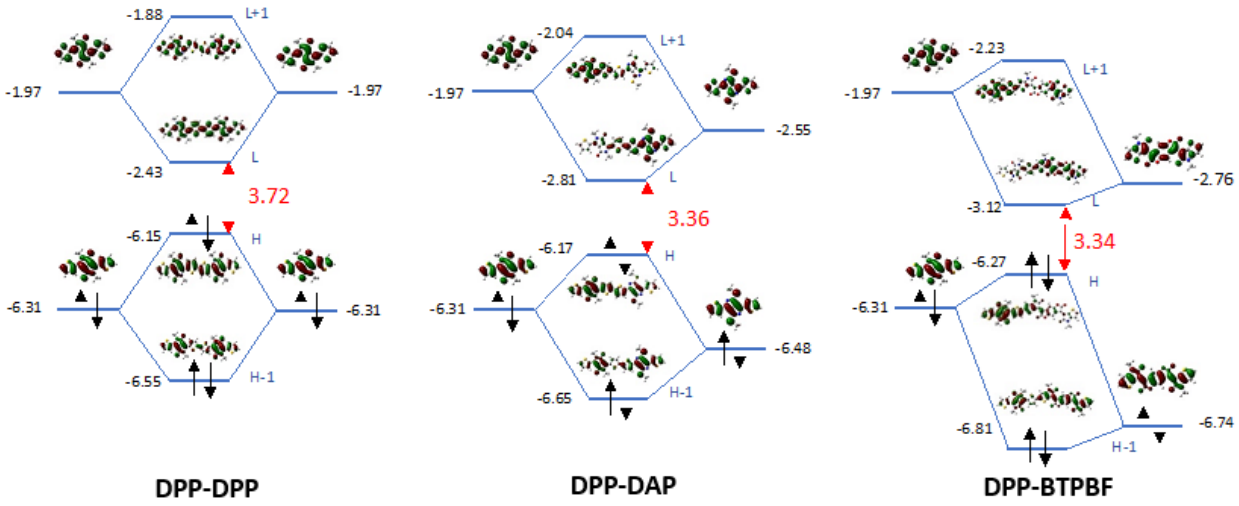

Figure 2. Energy levels (with values in eV) and shapes of frontier MOs of A-A′ dimers with A = DPP and A′ = DPP, DAP and BTPBF.

The energies (ΔE) and oscillator strengths associated with the $S_0 \rightarrow S_1$ electronic transition, as well as the quantities characterizing the spatial extent of the photo-induced charge transfer [58,59] (namely, the amount of charge transferred Δq, the charge transfer distance Δr, and the dipole moment variation $\Delta \mu$) are gathered in Table 1. Consistently with the values of HOMO-LUMO gaps, the transition energies of the A-A′ systems evolve in the order: DPP-DPP > DPP-DAP > DPP-BTBPF. As indicated by its largest oscillator strength, DPP-BTBPF also exhibited the highest light-harvesting efficiency, owing to the larger spatial extent of the photo-excitation compared with the two other systems. While the dipole moment variation was equal to zero in DPP-DPP owing to its symmetrical structure, DPP-DAP and DPP-BTPBF exhibited large $\Delta \mu$ values, which indicate a significant charge transfer from the DPP to the A′ moiety in these two systems.

Table 1. Characterization of the $S_0 \rightarrow S_1$ electron transition in DPP, DAP, and BTPBF monomers, as well as in DPP-DPP, DPP-DAP, and DPP-BTPBF A-A′ units: transition energies (ΔE, eV), wavelengths (λ, nm), oscillator strengths (f, dimensionless), amount of charge transferred ($|e|$), charge transfer distances (Å), and change in dipole moments (D).

System	ΔE	λ	f	Δq	Δr	$\Delta \mu$
DPP	2.69	461	0.532	0.310	0.001	0.002
DAP	2.41	516	0.506	0.736	0.003	0.006
BTPBF	2.37	524	0.856	0.436	0.003	0.006
DPP-DPP	2.28	544	1.817	0.358	0.007	0.012
DPP-DAP	2.12	589	1.677	0.410	2.844	5.604
DPP-BTPBF	2.03	610	1.860	0.481	3.320	7.673

The HOMO and LUMO energies, as well as the electronic gaps calculated for increasingly large $(A\text{-}A')_n$ oligomers are summarized in Table S3, while the optical properties are

gathered in Tables S4 and S5. To no surprise, as the conjugated oligomers increased in size, the electronic gap lowered as a result of the continuous destabilization of the HOMO and stabilization of the LUMO. Consistently, the optical gap decreased when increasing the conjugated chain length, while the oscillator strength increased. The evolution of the transition energies ΔE as a function of 1/N (with N the number of double bonds along the conjugated path) is shown in Figure 3. The transition energies extrapolated using Equation (1) are 1.82 eV for A′ = DPP, and 1.62 eV for DAP and BTPBF.

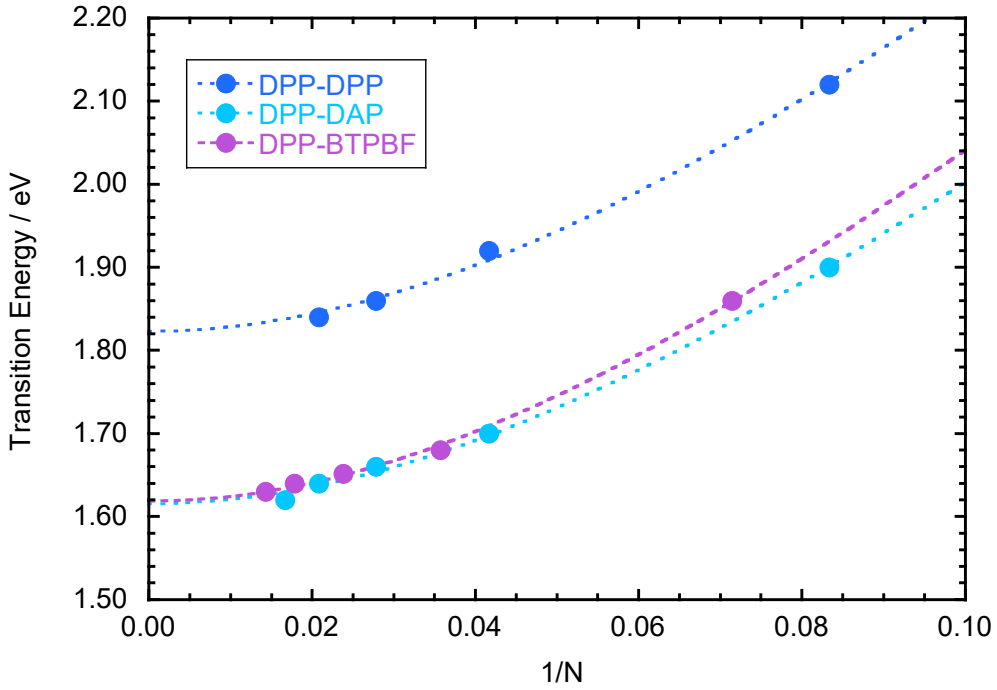

Figure 3. Evolution with chain length of the vertical transition energies of the $(A\text{-}A')_n$ oligomers, as calculated at the IEFPCM:M06-2X/6-311G(d) level in chlorobenzene. Lines are fits calculated according to equation 1. Optimized values of the Kuhn fit parameters E_0 and D_k are 6.63 eV and −0.92 for A′ = DPP, 6.10 eV and −0.93 for A′ = DAP, and 6.39 eV and −0.94 for A′ = BTPBF.

3.3. Opto-Electronic Properties of A-A′ Copolymers in Solution and in the Solid State

The optical properties of the different A-A′ copolymers P(DPP-DPPeH), P(DPP-DPPC12), P(DPP-DAP), and P(DPP-BTPBF) were studied by UV-vis-NIR absorption spectrophotometry in solution and in thin films (Table 2). As shown in Figure 4, all the copolymers display two characteristic bands. A first weakly absorbing band is located in the short-wavelength region, around 400 nm for P(DPP-DPPeH) and P(DPP-DPPC12) and 470 nm for P(DPP-DAP) and P(DPP-BTPBF). The second band is broad and covers different wavelength ranges depending on the comonomer. Both copolymers exclusively based on DPP, P(DPP-DPPeH), and P(DPP-DPPC12) absorbed in solution in the same range (500–900 nm) with a maximum absorption at 700 nm. However, a shoulder could be observed at 875 nm for the copolymer with the C12 linear chain, which can be related to the presence of aggregates in solution. As predicted by DFT calculations, copolymers based on DAP and BTPBF presented a large absorption shifted towards the infrared. P(DPP-DAP) exhibited an absorption from 530 nm up to around 1200 nm while P(DPP-BTPBF) absorbed from 650 to 1400 nm. These results suggest that the electron accepting strength of monomers evolves in the order DPP < DAP < BTPBF. From DPP to DAP, the gain towards the infrared was 140 nm for the maximum of absorption, and 295 nm for the band edge. When comparing DAP and BTPBF, the shift in maximum absorption was 209 nm and 225 nm for the band edge. This confirms that the BTPBF building block is a strong electron acceptor unit, allowing an absorption range between 700 and 1400 nm, with a maximum

absorption at 1050 nm. When combined with DTS instead of DPP, the absorption was even more shifted in the NIR by 50 nm.

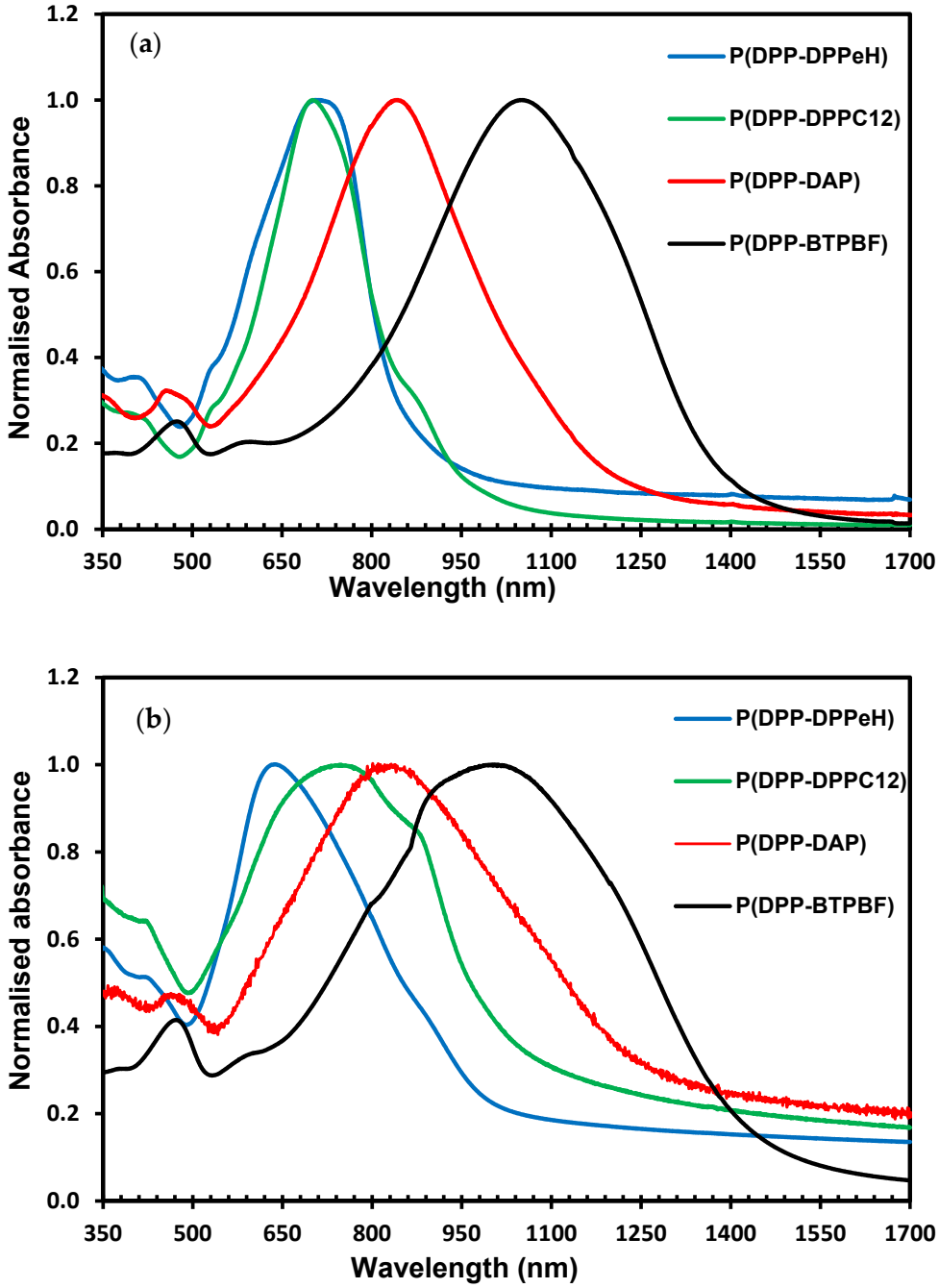

Figure 4. Normalized absorption spectra of A-A′ copolymers P(DPP-DPPeH), P(DPP-DPPC12), P(DPP-DAP), and P(DPP-BTPBF); (**a**) in chlorobenzene solutions; (**b**) in thin films (spin coated from chlorobenzene solutions).

The absorption spectra obtained with copolymers deposited as thin films slightly differ from those measured in solution. For copolymers only based on DPP, a redshift due to π-stacking was only observed with P(DPP-DPPC12), with a bathochromic effect of 47 nm for the maximum absorption and 60 nm for the band edge. It is also worth noting that the charge transfer band became broader with a strong increase of the shoulder at 875 nm, probably coming from the formation of aggregates or a more crystalline material. The change between solution and film was different in the case of P(DPP-DPPeH) that

bears an ethyl hexyl chain on every unit. Indeed, the maximum wavelength was blue shifted, probably due to the branched chains that hinder the molecular packing, while an enlargement of the main absorption band was observed with a shoulder at 850 nm. The charge transfer band was enlarged from solution to solid state, but the maximum absorption was blue shifted of 74 nm, whilst the band edge showed a redshift of 100 nm.

Table 2. Optoelectronic characteristics for monomers and copolymers.

	[a] λ_{max} (nm) Solution	[a] λ_{max} (nm) Solid State	[a] λ_{edge} (nm) Solid State	[a] E_g^{opt} (eV)	[b] HOMO (eV)	[b] LUMO (eV)	[b] E_g^{cv} (eV)
Monomers							
DPP	545	-	570 (solution)	2.13 [c]	−5.7	−3.5	2.2
DAP	565	-	640 (solution)	1.94 [c]	−5.4	−3.6	1.7
BTPBF	695	-	775 (solution)	1.60 [c]	−5.3	−4.0	1.3
Copolymers							
P(DPP-DPPeH)	706	632	980	1.35	−5.4	−4.0	1.4
P(DPP-DPPC12)	701	748	1030	1.3	−5.5	−4.1	1.3
P(DPP-DAP)	842	839	1230	1.1	−5.4	−4.2	1.2
P(DPP-BTPBF)	1051	1047	1450	0.9	−5.5	−4.4	0.9
P(DTS-DPPeH)	795	800	1000	1.3	−5.4	−3.9	1.5
P(DTS-DAP)	837	867	1180	1.1	−5.4	−4.1	1.3
P(DTS-BTPBF)	1100	1081	1440	0.9	−5.2	−4.2	1.0

[a]: spectrophotometry; [b]: cyclovoltammetry; *c* measured by spectrophotometry in chloroform. E_g^{opt} is estimated from the edge of absorption bands in solid state. E_{HOMO} (eV) = $-E^{onset}$ (ox) − 4.70 (eV); E_{LUMO} (eV) = $-E^{onset}$(red) − 4.70 (eV).

For P(DPP-DAP) and P(DPP-BTPBF), the maximum of absorption was not really shifted between solution and solid state; only a redshift of the band edge of around 50 nm was observed, indicating that aggregates can be already formed in solution.

All these spectra allowed the calculation of optical bandgaps of 1.3, 1.2, 1.0, and 0.9 eV for P(DPP-DPPeH), P(DPP-DPPC12), P(DPP-DAP), and P(DPP-BTPBF), respectively. These band gaps are very small and quite similar to that of the corresponding D-A copolymers reported in our previous publication with DTS as donor unit (reported in Table 2 for comparison) [47]. In order to investigate further the effects of alternating two acceptor monomers on the electronic levels, HOMO and LUMO levels were determined by cyclic voltammetry.

A direct comparison of A-A′ copolymers to D-A, with the evolution of band gaps, HOMO and LUMO levels are presented as a summary in the SI, Table S6.

Polymers have been drop-casted onto a platinum electrode from chlorobenzene solutions (10 mg mL^{-1}), and submitted to cyclic voltammetry in dry acetonitrile with Bu_4NPF_6 as the supporting electrolyte (see voltammograms in SI, Figures S8–S11). The HOMO and LUMO levels (in eV, ref vacuum) of copolymers were deduced from the oxidation and reduction potentials (see Table 2). For comparison, the DPP, DAP, and BTPBF monomers were also analyzed by cyclic voltammetry in the same conditions. Results previously obtained with analogous D-A′ copolymers are also reported in Table 2.

The HOMO-LUMO band gap determined with monomers showed a strong decrease in the order DPP, DAP, and BTBPF (2.2, 1.8, and 1.3 eV, respectively). Both HOMO and LUMO levels were affected by changing the structure. All these energy levels are reported in Figure 5, and presented with poly(3-hexylthiophene) (P3HT) and PCBM, for comparison. When comparing the A-A′ copolymers, the main observation is that LUMO levels were deepened in correlation with the electron affinity of the comonomer combined with DPP, as it was already observed when copolymerized with DTS. HOMO levels were only slightly modified and were about −5.0 eV on average. When comparing the series of P(DTS-A) copolymers to P(DPP-A) copolymers with the same A, replacing DTS by DPP provoked the lowering of both LUMO and HOMO levels in the same manner, leading to unmodified bandgaps, as already observed with optical gaps. In the case of P(DTS-BTPBF) and P(DPP-BTPBF) also, the change of DTS by DPP strongly affected both HOMO and LUMO levels

by roughly 0.25 eV, leading to deeper levels without perturbating the bandgaps. Thus, the P(DPP-BTPBF) copolymer exhibited very deep HOMO and LUMO levels at −5.5 and −4.4 eV, respectively.

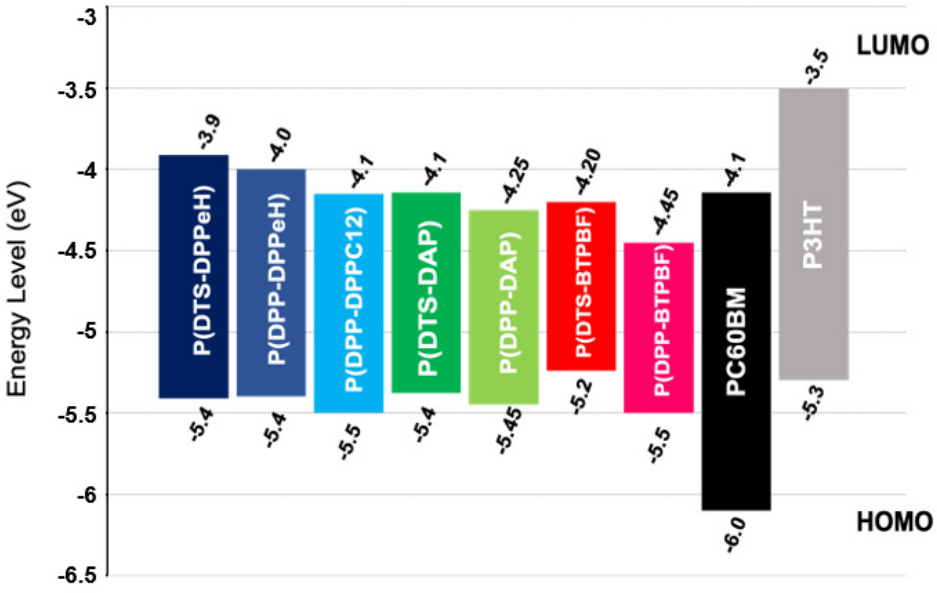

Figure 5. HOMO-LUMO energy levels of the copolymers (A-A') based on DPP and (D-A) based on DTS determined by cyclic voltammetry.

3.4. Thermal Properties of A-A' Copolymers

The thermal stability of polymers is an important parameter when applied to electronic devices. It was studied for all the A-A' copolymers by thermogravimetric analysis, under nitrogen between 0 °C and 600 °C, with a heating rate of 10 °C min^{-1} (Figure 6).

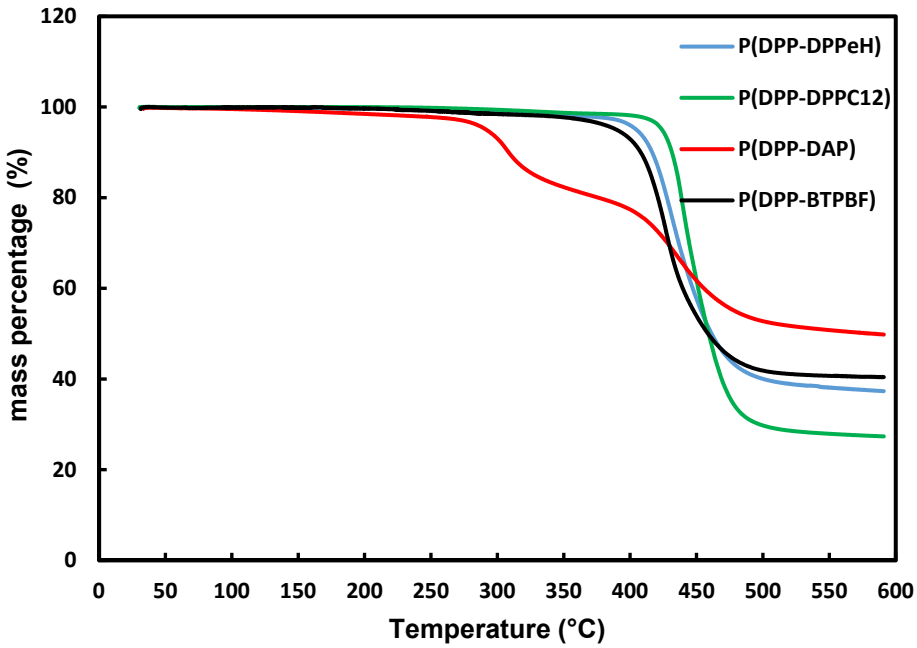

Figure 6. TGA of copolymers P(DPP-DPPeH), P(DPP-DPPC12), P(DPP-DAP), and P(DPP-BTPBF) with a heating ramp of 10 °C min^{-1} up to 600 °C under N_2 flux.

All copolymers were stable up to at least 350 °C, except P(DPP-DAP), which exhibited two steps of degradation starting at 250 °C. For the latter, the first step of degradation

occurred from 250 °C to 400 °C with a weight loss of around 20%. The second weight loss of an additional 30% finished at 500 °C. This early degradation was also observed with P(DTS-DAP) (see SI, Figure S12) and can be related to a weaker stability of the ethylhexyl chains when connected to the sulfur atom as in the DAP unit. The weight loss of around 20% is in agreement with the theoretical weight percentage of 21% expected for both ethylhexyl chains in the repeating unit constituted of DPP and DAP. For the copolymers P(DPP-DPPeH), P(DPP-DPPC12), and P(DPP-BTPBF), the thermograms showed one step of degradation, with a weight loss of 60%, 70%, and 59%, respectively. These variations can be roughly related to the molar mass of the alkyl chains present on the DPPeH, DPPC12, and BTPBF units.

For comparison, the corresponding D-A′ copolymers exhibited a similar degradation temperature around 400 °C, except for P(DTS-DAP) that also presented a lower degradation temperature of 200 °C, with an observed weight loss of around 20%, in agreement with an expected one of 23% in the repeating unit DTS-DAP (see SI, Figures S12 and S13). The thermal properties of P(DPP-DPPeH), P(DPP-DPPC12), P(DPP-DAP), and P(DPP-BTPBF) copolymers were also examined by differential scanning calorimetry (DSC). The DSC thermograms for copolymers are shown in the SI, Figures S14–S17 for P(DPP-DPPeH), P(DPP-DPPC12), P(DPP-DAP), and P(DPP-BTPBF), respectively. For all copolymers, DSC thermograms did not show any clear thermal transition up to 300 °C, even if a slight difference was observed between the first and second cycle. The absence of a melting point suggests that these polymers either tend to form an amorphous phase or that the melting temperature is above 300 °C. The size of the crystal domains may also be too small to be detected.

4. Conclusions

In this article, we paid particular attention to a limited reported strategy in the literature to synthesize A-A′ low bandgap copolymers, combining DPP with itself or with the two highly electro-deficient monomer units DAP and BTPBF. Stille coupling copolymerization was applied to the synthesis of the alternating copolymers P(DPP-DPPeH), P(DPP-DPPC12), P(DPP-DAP), and P(CPDT-BTPBF). The synthesis of these copolymers required optimizations in terms of reaction conditions such as temperature, time, and reaction solvent in order to acquire soluble materials. Subsequently, the resulting copolymers were analyzed by UV-VIS-NIR spectrophotometry in solution and in solid state. When DPP was replaced by its derivative DAP or by BTPBF, which are much more electro-deficient monomers, a strong redshift of the global absorption was observed, thus accompanied by a decrease of the optical bandgap of 0.2 and 0.5 eV, respectively. These optical properties were in agreement with computational results which showed that transition energies of the A-A′ copolymers evolve in the order: DPP-DPP > DPP-DAP > DPP-BTBPF. Moreover, electrochemical measurements provided insights on how HOMO and LUMOs levels are impacted by the nature of the A′ unit, and more generally on the interest of designing A-A′ copolymers in comparison with D-A′ ones. Indeed, despite D-A′ and A-A′ copolymers displaying similar optical bandgaps, HOMO and LUMO levels were deepened for the latter by an average absolute value of 0.25 eV. The most significant changes were obtained with the BTPBF unit, leading to a P(DPP-BTPBF) with very low electronic levels at −5.5 and −4.4 eV for HOMO and LUMO, respectively. Finally, the thermal properties of the four copolymers are suitable for optoelectronic applications since their degradation onset temperatures were above 250 °C.

Supplementary Materials: The following supporting information can be downloaded at: https://www.mdpi.com/article/10.3390/app12094494/s1, Figure S1: ^{1}H NMR spectrum of di-bromoBTPBF (400 MHz, $CDCl_3$); Figure S2: ^{1}H NMR spectra of P(DPP-DPPeH) (400 MHz, TCE, 125 °C); Figure S3: ^{1}H NMR spectra of P(DPP-DPPC12) (400 MHz, TCE, 125 °C); Figure S4: ^{1}H NMR spectrum of P(DPP-DAP) (400 MHz, TCE, 125 °C); Figure S5: ^{1}H NMR spectrum of P(DPP-BTPBF) (400 MHz, TCE, 125 °C); Figure S6: Optimized geometries of DPP (top) and DAP (middle) with the lateral tetrahydrothiophene groups in anti (a,c) and syn (b,d) positions, and optimized structure of BTPBF (e);

Figure S7: Optimized geometries of $(DPP\text{-}DPP)_2$ (a,d), $(DPP\text{-}DAP)_2$ (b,e), and $(DPP\text{-}BTPBF)_2$ (c,f) in their anti (top) and syn (bottom) configurations; Figure S8: Cyclic voltammograms of P(DPP-DPPeH) in 0.1 M Bu_4NPF_6/CH_3CN using a sweep rate of 0.1 V s^{-1}; Figure S9: Cyclic voltammograms of P(DPP-DPPC12) in 0.1 M Bu_4NPF_6/CH_3CN using a sweep rate of 0.1 V s^{-1}; Figure S10: Cyclic voltammograms: reduction (left) and oxidation (right) of P(DPP-DAP) in 0.1 M Bu_4NPF_6/CH_3CN using a sweep rate of 0.1 V s^{-1}; Figure S11: Cyclic voltammograms: reduction (left) and oxidation (right) of P(DPP-BTPBF) in 0.1 M Bu_4NPF_6/CH_3CN using a sweep rate of 0.1 V s^{-1}; Figure S12: Thermograms of P(DTS-DPP) and P(DTS-DAP) with a heating rate of 10 °C min^{-1} under nitrogen; Figure S13: Thermogram of P(DTS-BTPBF) with a heating rate of 10 °C min^{-1} under nitrogen; Figure S14: DSC thermogram of P(DPP-DPPeH) with a heating ramp of 10 °C min^{-1}; Figure S15: DSC thermogram of P(DPP-DPPC12) with a heating ramp of 10 °C min^{-1}. Figure S16: DSC thermogram of P(DPP-DAP) with a heating ramp of 10 °C min^{-1}; Figure S17: DSC thermogram of P(DPP-BTPBF) with a heating ramp of 10 °C min^{-1}; Table S1: Relative Gibbs free energy between *syn* and *anti* configurations calculated for $(A\text{-}A')_2$ dimers at the M06-2X/6-311G(d) level in the gas phase; Table S2: HOMO and LUMO energies and gaps 〚ΔE〛 g = E_LUMO-E_HOMO (all values in eV) calculated for monomers and A-A' units at the M06-2X/6-311G(d) level; Table S3: HOMO and LUMO energies and gaps 〚ΔE〛 g = E_LUMO-E_HOMO (all values in eV) calculated for increasingly large oligomers at the M06-2X/6-311G(d) level; Table S4: Characterization of the $S_0 \rightarrow S_1$ electron transition in increasingly large D-A oligomers, as calculated at the M06-2X/6-311G(d) level in the gas phase. Transition energies (eV), wavelengths (nm), oscillator strengths (dimensionless), amount of charge transferred (|e|), charge transfer distances (Å), and change in dipole moments (D); Table S5: Characterization of the $S_0 \rightarrow S_1$ electron transition in increasingly large D-A oligomers, as calculated at the IEFPCM:M06-2X/6-311G(d) level in chlorobenzene. Transition energies (eV), wavelengths (nm), oscillator strengths (dimensionless), amount of charge transferred (|e|), charge transfer distances (Å), and change in dipole moments (D); Table S6: Comparison of optoelectronic properties of A-A' copolymers (bold) to D-A analogous copolymer; λ_{max}, λ_{edge} and E_g^{opt} were obtained from UV-Visible-NIR absorption spectra; E_g^{cv}, HOMO and LUMO levels were estimated from cyclovoltammetry measurements.

Author Contributions: Conceptualization, C.L.-D. and A.B.; investigation, W.K., H.A., S.B., G.H.R., B.O. and F.C.; resources, C.L.-D., A.B. and L.H.; writing—original draft preparation, W.K., F.C. and C.L.-D.; writing—review and editing, C.L.-D.; visualization, W.K. and C.L.-D.; supervision, A.B. and C.L.-D.; project administration, C.L.-D., A.B. and L.H.; funding acquisition, L.H. and C.L.-D. All authors have read and agreed to the published version of the manuscript.

Funding: This research was funded by the AgenceNationale de la Recherche (TAPIR project no. ANR-15-CE24-0024-02), the Région Nouvelle Aquitaine (TAMANOIR project no. 2016-1R10105-0007207) and E2S-UPPA (technology transfer project PIROETT).

Institutional Review Board Statement: Not applicable.

Informed Consent Statement: Not applicable.

Data Availability Statement: Not applicable.

Acknowledgments: Computer time was provided by the Pôle Modélisation HPC facilities of theInstitut des Sciences Moléculaires, cofunded by the Nouvelle Aquitaine region, as well as by the MCIA (Mésocentre de CalculIntensifAquitain) resources of the Université de Bordeaux and of the Université de Pau et des Pays de l'Adour.

Conflicts of Interest: The authors declare no conflict of interest.

References

1. Chochos, C.L.; Choulis, S.A. How the structural deviations on the backbone of conjugated polymers influence their optoelectronic properties and photovoltaic performance. *Prog. Polym. Sci.* **2011**, *36*, 1326–1414. [CrossRef]
2. Heumueller, T.; Mateker, W.R.; Distler, A.; Fritze, U.F.; Cheacharoen, R.; Nguyen, W.H.; Biele, M.; Salvador, M.; von Delius, M.; Egelhaaf, H.-J.; et al. Morphological and electrical control of fullerene dimerization determines organic photovoltaic stability. *Energy Environ. Sci.* **2016**, *9*, 247–256. [CrossRef]
3. Distler, A.; Sauermann, T.; Egelhaaf, H.-J.; Rodman, S.; Waller, D.; Cheon, K.S.; Lee, M.; Drolet, N.; Guldi, D.M. The Effect of PCBM Dimerization on the Performance of Bulk Heterojunction Solar Cells. *Adv. Energy Mater.* **2014**, *4*, 1300693. [CrossRef]

4. Pont, S.; Osella, S.; Smith, A.; Marsh, A.V.; Li, Z.; Beljonne, D.; Cabral, J.T.; Durrant, J.R. Evidence for Strong and Weak Phenyl-C61-Butyric Acid Methyl Ester Photodimer Populations in Organic Solar Cells. *Chem. Mater.* **2019**, *31*, 6076–6083. [CrossRef]
5. Holliday, S.; Li, Y.; Luscombe, C.K. Recent advances in high performance donor-acceptor polymers for organic photovoltaics. *Prog. Polym. Sci.* **2017**, *70*, 34–51. [CrossRef]
6. Yoo, S.; Shin, E.-Y.; Cho, N.-K.; Park, S.; Woo, H.-Y.; Son, H.-J. Progress in morphology control from fullerene to nonfullerene acceptors for scalable high-performance organic photovoltaics. *J. Mater. Chem. A* **2021**, *9*, 24729–24758.
7. Chochos, C.L.; Tagmatarchis, N.; Gregoriou, V.G. Rational design on n-type organic materials for high performance organic photovoltaics. *RSC Adv.* **2013**, *3*, 7160–7181. [CrossRef]
8. Facchetti, A. π-Conjugated Polymers for Organic Electronics and Photovoltaic Cell Applications. *Chem. Mater.* **2011**, *23*, 733–758. [CrossRef]
9. Cho, S.; Lee, J.; Tong, M.H.; Seo, J.H.; Yang, C. Poly (diketopyrrolopyrrole-benzothiadiazole) with Ambipolarity Approaching 100% Equivalency. *Adv. Funct. Mater.* **2011**, *21*, 1910–1916. [CrossRef]
10. Guo, X.; Kim, F.S.; Seger, M.J.; Enekhe, J.S.A.; Watson, M.D. Naphthalene Diimide-Based Polymer Semiconductors: Synthesis, Structure–Property Correlations, and n-Channel and Ambipolar Field-Effect Transistors. *Chem. Mater.* **2012**, *24*, 1434–1442. [CrossRef]
11. Facchetti, A. Polymer donor–polymer acceptor (all-polymer) solar cells. *Mater. Today* **2013**, *16*, 123–132. [CrossRef]
12. Gao, L.; Zhang, Z.-G.; Xue, L.; Min, J.; Zhang, J.; Wei, Z.; Li, Y. All-Polymer Solar Cells Based on Absorption-Complementary Polymer Donor and Acceptor with High Power Conversion Efficiency of 8.27%. *Adv. Mater.* **2016**, *28*, 1884–1890. [CrossRef] [PubMed]
13. Liu, S.; Song, X.; Thomas, S.; Kan, Z.; Cruciani, F.; Laquai, F.; Bredas, J.-L.; Beaujuge, P.M. Thieno [3,4-c] Pyrrole-4,6-Dione-Based Polymer Acceptors for High Open-Circuit Voltage All-Polymer Solar Cells. *Adv. Energy Mater.* **2017**, *7*, 1602574. [CrossRef]
14. Jiang, X.; Xu, Y.; Wang, X.; Yang, F.; Zhang, A.; Li, C.; Ma, W.; Li, W. Conjugated polymer acceptors based on fused perylene bisimides with a twisted backbone for non-fullerene solar cells. *Polym. Chem.* **2017**, *8*, 3300–3306. [CrossRef]
15. Yang, J.; Xiao, B.; Tajima, K.; Nakano, M.; Takimiya, K.; Tang, A.; Zhou, E. Comparison among Perylene Diimide (PDI), Naphthalene Diimide (NDI), and Naphthodithiophene Diimide (NDTI) Based n-Type Polymers for All-Polymer Solar Cells Application. *Macromolecules* **2017**, *50*, 3179–3185. [CrossRef]
16. Zhou, E.; Nakano, M.; Izawa, S.; Cong, J.; Osaka, I.; Takimiya, K.; Tajima, K. All-Polymer Solar Cell with High Near-Infrared Response Based on a Naphthodithiophene Diimide (NDTI) Copolymer. *ACS Macro Lett.* **2014**, *3*, 872–875. [CrossRef]
17. Zhang, Z.-G.; Yang, Y.; Yao, J.; Xue, L.; Chen, S.; Li, X.; Morrison, W.; Yang, C.; Li, Y. Constructing a Strongly Absorbing Low-Bandgap Polymer Acceptor for High-Performance All-Polymer Solar Cells. *Angew. Chem. Int. Ed.* **2017**, *56*, 13503–13507. [CrossRef]
18. Guo, Y.-K.; Li, Y.-K.; Han, H.; Yan, H.; Zhao, D. All-Polymer Solar Cells with Perylenediimide Polymer Acceptors. *Chin. J. Polym. Sci.* **2017**, *35*, 293–301. [CrossRef]
19. Zhou, Y.; Yan, Q.; Zheng, Y.-Q.; Wang, J.-Y.; Zhao, D.; Pei, J. New polymer acceptors for organic solar cells: The effect of regio-regularity and device configuration. *J. Mater. Chem. A* **2013**, *1*, 6609–6613. [CrossRef]
20. Zhang, Y.; Guo, X.; Su, W.; Guo, B.; Xu, Z.; Zhang, M.; Li, Y. Perylene diimide-benzodithiophene D-A copolymers as acceptor in all-polymer solar cells. *Org. Electron.* **2017**, *41*, 49–55. [CrossRef]
21. Dai, S.; Cheng, P.; Lin, Y.; Wang, Y.; Ma, L.; Ling, Q.; Zhan, X. Perylene and naphthalene diimide polymers for all-polymer solar cells: A comparative study of chemical copolymerization and physical blend. *Polym. Chem.* **2015**, *6*, 5254–5263. [CrossRef]
22. Guo, Y.; Li, Y.; Awartani, O.; Han, H.; Zhao, J.; Ade, H.; Yan, H.; Zhao, D. Improved Performance of All-Polymer Solar Cells Enabled by Naphthodiperylenetetraimide-Based Polymer Acceptor. *Adv. Mater.* **2017**, *29*, 1700309. [CrossRef] [PubMed]
23. Wei, R.; Chen, H.; Guo, Y.; Han, H.; Zhang, D.; Zhu, Y.; He, F.; Zhao, D. Thiophene-Fused Perylenediimide-Based Polymer Acceptors for High-Performance All-Polymer Solar Cells. *Macromolecules* **2021**, *54*, 1499–1506. [CrossRef]
24. Hendriks, K.H.; Li, W.; Wienk, M.M.; Janssen, R.A.J. Small-Bandgap Semiconducting Polymers with High Near-Infrared Photoresponse. *J. Am. Chem. Soc.* **2014**, *136*, 12130–12136. [CrossRef] [PubMed]
25. Lim, D.-H.; Ha, J.-W.; Choi, H.; Yoon, S.C.; Lee, B.R.; Ko, S.-J. Recent progress of ultra-narrow-bandgap polymer donors for NIR-absorbing organic solar cells. *Nanoscale Adv.* **2021**, *3*, 4306–4320. [CrossRef]
26. Verstraeten, F.; Gielen, S.; Verstappen, P.; Raymakers, J.; Penxten, H.; Lutsen, L.; Vandewal, K.; Maes, W. Efficient and readily tuneable near-infrared photodetection up to 1500 nm enabled by thiadiazoloquinoxaline-based push-pull type conjugated polymers. *J. Mater. Chem. C* **2020**, *8*, 10098–10103. [CrossRef]
27. Qian, G.; Qi, J.; Wang, Z.Y. Synthesis and study of low-bandgap polymers containing the diazapentalene and diketopyrrolopyrrole chromophores for potential use in solar cells and near-infrared photodetectors. *J. Mater. Chem.* **2012**, *22*, 12867–12873. [CrossRef]
28. Zhao, X.; Wen, Y.; Ren, L.; Ma, L.; Liu, Y.; Zhan, X. An acceptor-acceptor conjugated copolymer based on perylene diimide for high mobility n-channel transistor in air. *J. Polym. Sci. Part A Polym. Chem.* **2012**, *50*, 4266–4271. [CrossRef]
29. Gwinner, M.C.; Brenner, T.J.K.; Lee, J.-K.; Newby, C.; Ober, C.K.; McNeil, C.R.; Sirringhaus, H. Organic field-effect transistors and solar cells using novel high electron-affinity conjugated copolymers based on alkylbenzotriazole and benzothiadiazole. *J. Mater. Chem.* **2012**, *22*, 4436–4439. [CrossRef]

30. Banal, J.L.; Subbiah, J.; Graham, H.; Lee, J.-K.; Ghiggino, K.P.; Wong, W.W.H. Electron deficient conjugated polymers based on benzotriazole. *Polym. Chem.* **2013**, *4*, 1077–1083. [CrossRef]
31. Stalder, R.; Mei, J.; Subbiah, J.; Grand, C.; Estrada, L.A.; So, F.; Reynolds, J.R. n-Type Conjugated Polyisoindigos. *Macromolecules* **2011**, *44*, 6303–6310. [CrossRef]
32. Ge, C.-W.; Mei, C.-Y.; Ling, J.; Wang, J.-T.; Zhao, F.-G.; Liang, L.; Li, H.-J.; Xie, Y.-S.; Li, W.-S. Acceptor–acceptor conjugated copolymers based on perylenediimide and benzothiadiazole for all-polymer solar cells. *J. Polym. Sci. Part A Polym. Chem.* **2014**, *52*, 1200–1215. [CrossRef]
33. Du, J.; Hu, K.; Zhang, J.; Meng, L.; Yue, J.; Angunawela, I.; Yan, H.; Qin, S.; Kong, X.; Zhang, Z.; et al. Polymerized small molecular acceptor based all-polymer solar cells with an efficiency of 16.16% via tuning polymer blend morphology by molecular design. *Nat. Commun.* **2021**, *12*, 5264. [CrossRef]
34. Zhao, X.; Wang, T.; Wang, W.; Sun, R.; Wu, Q.; Shen, H.; Xia, J.; Wang, Y.; Zhang, M.; Min, J. Polymerized small-molecule acceptors based on vinylene as π-bridge for efficient all-polymer solar cells. *Polymer* **2021**, *230*, 124104–124110. [CrossRef]
35. Yuen, J.D.; Fan, J.; Seifter, J.; Lim, B.; Hufschmid, R.; Heeger, A.J.; Wudl, F. High Performance Weak Donor–Acceptor Polymers in Thin Film Transistors: Effect of the Acceptor on Electronic Properties, Ambipolar Conductivity, Mobility, and Thermal Stability. *J. Am. Chem. Soc.* **2011**, *133*, 20799–20807. [CrossRef] [PubMed]
36. Hasegawa, T.; Ashizawa, M.; Hiyoshi, J.; Kawauchi, S.; Mei, J.; Bao, Z.; Matsumoto, H. An ultra-narrow bandgap derived from thienoisoindigo polymers: Structural influence on reducing the bandgap and self-organization. *Polym. Chem.* **2016**, *7*, 1181–1190. [CrossRef]
37. Wang, K.; Huang, J.; Ko, J.; Leong, W.L.; Wang, M. Direct arylation polymerization toward ultra-low bandgap poly (thienoisoindigo-alt-diketopyrrolepyrrole) conjugated polymers: The effect of β-protection on the polymerization and properties of the polymers. *J. Polym. Sci. Part A Polym. Chem.* **2017**, *55*, 3205–3213. [CrossRef]
38. Zhang, C.; Chen, Z.; Zeng, W.; Yu, G.; Yang, C. Narrow band-gap copolymers with two acceptors of benzo [1,2-c;3,4-c′] bis [1,2,5] thiadiazole and Benzo [c] [1,2,5] thiadiazole: Synthesis, characteristics and application in field-effect transistors. *Dye. Pigment.* **2016**, *130*, 291–297. [CrossRef]
39. Li, Y.; Sonar, P.; Murphy, L.; Honga, W. High mobility diketopyrrolopyrrole (DPP)-based organic semiconductor materials for organic thin film transistors and photovoltaics. *Energy Environ. Sci.* **2013**, *6*, 1684–1710. [CrossRef]
40. Liu, Q.; Bottle, S.E.; Sonar, P. Developments of Diketopyrrolopyrrole-Dye-Based Organic Semiconductors for a Wide Range of Applications in Electronics. *Adv. Mater.* **2019**, *36*, 1903882. [CrossRef]
41. Luo, N.; Zhang, G.; Liu, Z. Keep glowing and going: Recent progress in diketopyrrolopyrrole synthesis towards organic optoelectronic materials. *Org. Chem. Front.* **2021**, *8*, 4560–4581. [CrossRef]
42. Luo, N.; Ren, P.; Feng, Y.; Shao, X.; Zhang, H.-L.; Liu, Z. Side-Chain Engineering of Conjugated Polymers for High-Performance Organic Field-Effect Transistors. *J. Phys. Chem. Lett.* **2022**, *13*, 1131–1146. [CrossRef] [PubMed]
43. Khelifi, W.; Awada, H.; Brymora, K.; Blanc, S.; Hirsch, L.; Castet, F.; Bousquet, A.; Lartigau-Dagron, C. Halochromic Switch from the 1st to 2nd Near-Infrared Window of Diazapentalene–Dithienosilole Copolymers. *Macromolecules* **2019**, *52*, 4820–4827. [CrossRef]
44. Zhang, G.; Ye, Z.; Li, P.; Guo, J.; Wang, Q.; Tang, L.; Lua, H.; Qiu, L. A new thieno-isoindigo derivative-based D–A polymer with very low bandgap for high-performance ambipolar organic thin-film transistors. *Polym. Chem.* **2015**, *6*, 3970–3978. [CrossRef]
45. Zhang, G.; Chen, J.; Dai, Y.; Song, S.; Ye, Z.; Lu, H.; Qiu, L.; Cho, K. Synthesis and optimization solid-state order using side-chain position of thieno-isoindigo derivative-based D–A polymers for high-performance ambipolar organic thin films transistors. *Dye. Pigment.* **2017**, *137*, 221–228. [CrossRef]
46. Cao, Y.; Dou, J.-H.; Zhao, N.-J.; Zhang, S.; Zheng, Y.-Q.; Zhang, J.-P.; Wang, Y.-Y.; Pei, J.; Wang, Y. Highly Efficient NIR-II Photothermal Conversion Based on an Organic Conjugated Polymer. *Chem. Mater.* **2017**, *29*, 718–725. [CrossRef]
47. Brymora, K.; Khelifi, W.; Awada, H.; Blanc, S.; Hirsch, L.; Bousquet, A.; Lartigau-Dagron, C.; Castet, F. Comprehensive theoretical and experimental study of near infrared absorbing copolymers based on dithienosilole. *Polym. Chem.* **2020**, *11*, 3637–3643. [CrossRef]
48. Gierschner, J.; Cornil, J.; Egelhaaf, H.J. Optical Bandgaps of π-Conjugated Organic Materials at the Polymer Limit: Experiment and Theory. *Adv. Mater.* **2007**, *19*, 173–191. [CrossRef]
49. Wykes, M.; Milián-Medina, B.; Gierschner, J. Computational engineering of low bandgap copolymers. *Front. Chem.* **2013**, *1*, 1–12. [CrossRef]
50. Oliveira, E.F.; Roldao, J.C.; Milián-Medina, B.; Lavarda, F.C.; Gierschner, J. Calculation of low bandgap homopolymers: Comparison of TD-DFT methods with experimental oligomer series. *J. Chem. Phys. Lett.* **2016**, *645*, 169–173. [CrossRef]
51. Torras, J.; Casanovas, J.; Alemán, C. Reviewing Extrapolation Procedures of the Electronic Properties on the π-Conjugated Polymer Limit. *J. Phys. Chem. A* **2012**, *116*, 7571–7583. [CrossRef] [PubMed]
52. Karsten, B.P.; Viani, L.; Gierschner, J.; Cornil, J.; Janssen, R.A.J. An Oligomer Study on Small Band Gap Polymers. *J. Phys. Chem. A* **2008**, *112*, 10764–10773. [CrossRef] [PubMed]
53. Zhao, Y.; Truhlar, D.G. The M06 suite of density functionals for main group thermochemistry, thermochemical kinetics, noncovalent interactions, excited states, and transition elements: Two new functionals and systematic testing of four M06-class functionals and 12 other functionals. *Theor. Chem. Acc.* **2008**, *120*, 215–241.

54. Sancho-García, J.C.; Pérez-Jiménez, A.J. Improved accuracy with medium cost computational methods for the evaluation of bond length alternation of increasingly long oligoacetylenes. *Phys. Chem. Chem. Phys.* **2007**, *9*, 5874–5879. [CrossRef]
55. Torrent-Sucarrat, M.; Navarro, S.; Cossío, F.P.; Anglada, J.M.; Luis, J.M. Relevance of the DFT method to study expanded porphyrins with different topologies. *J. Comput. Chem.* **2017**, *38*, 2819–2828. [CrossRef]
56. Tomasi, J.; Mennucci, B.; Cammi, R. Quantum Mechanical Continuum Solvation Models. *Chem. Rev.* **2005**, *105*, 2999–3094. [CrossRef]
57. Kuhn, W. About the absorption spectrum of the polyenes. *Helv. Chim. Acta* **1948**, *31*, 1780–1799. [CrossRef]
58. Le Bahers, T.; Adamo, C.; Ciofini, I. A Qualitative Index of Spatial Extent in Charge-Transfer Excitations. *J. Chem. Theory Comput.* **2011**, *7*, 2498–2506.
59. Ciofini, I.; Le Bahers, T.; Adamo, C.; Odobel, F.; Jacquemin, D. An all-atom empirical energy function for the simulation of nucleic acids. *J. Phys. Chem. C* **2012**, *116*, 11946–11955. [CrossRef]